Proton conduction in hydronium solvate ionic liquids affected by ligand shape

AUTHOR(S):

Kawata, Kio; Kitada, Atsushi; Tsuchida, Naoki; Saimura, Masayuki; Nagata, Takashi; Katahira, Masato; Fukami, Kazuhiro; Murase, Kuniaki

ARTICLE

Proton conduction in hydronium solvate ionic liquids affected by ligand shape

Received 00th January 20xx,
Accepted 00th January 20xx

DOI: 10.1039/x0xx00000x

Kio Kawata,[a] Atsushi Kitada,*[a] Naoki Tsuchida,[a] Masayuki Saimura,[b] Takashi Nagata,[b] Masato Katahira,[b] Kazuhiro Fukami [a] and Kuniaki Murase [a]

We investigated the ligand dependence of the proton conduction of hydronium solvate ionic liquids (ILs), consisting of hydronium ion (H_3O^+), polyether ligands, and bis[(trifluoromethyl)sulfonyl]amide anion (Tf_2N^-; Tf = CF_3SO_2). The ligands were changed from previously reported 18-crown-6 (18C6) to other cyclic or acyclic polyethers, namely, dicyclohexano-18-crown-6 (Dh18C6), benzo-18-crown-6 (B18C6) and pentaethylene glycol dimethyl ether (G5). Pulsed-field gradient spin echo nuclear magnetic resonance results revealed that the protons of H_3O^+ move faster than those of cyclic 18C6-based ligands but as fast as those of acyclic G5 ligands. Based on these results and density functional theory calculations, we propose that coordination of cyclic ether ligand to H_3O^+ ion is essential for fast proton conduction in hydronium solvate ILs. Our results attract special interest for many electro- and bio-chemical applications such as electrolyte systems for fuel cells and artificial ion channels for biological cells.

Introduction

When two or more substances are mixed, the properties of the mixture can drastically change from those of pure substance. Moreover, even a slight structural change in one of the components can significantly affect the properties, which donate the designability of functions. The neutralization of Brønsted or Lewis acids and bases often results in ionization, e.g. dissociation, protonation, solvation, and complexation. Sometimes, the acid-base mixtures can be classified as ionic liquids (ILs), which are defined as salts that melt below 100 °C. ILs show various characteristics, such as high ionic conductivity, high chemical and thermal stability, and solubility. Consequently, ILs have received significant attention as media for chemical, biochemical, and electrochemical systems.[1–6]

ILs can be classified into four types: solvate ILs, protic ILs, aprotic ILs, and inorganic ILs.[7] We previously reported a hydronium (H_3O^+) solvate IL $[H_3O^+{\cdot}18C6]Tf_2N$ (18C6 = 18-crown-6; Tf_2N = bis[(trifluoromethyl)sulfonyl]amide, Tf = SO_2CF_3) as the first example of a molten salt of $[H_3O^+{\cdot}ligand]$ complex,[8] while other groups had been reported solid state $[H_3O^+{\cdot}ligand]$ complexes using common anions (e.g. ClO_4^-, SbF_6^-, PF_6^-, TfO^-, BF_4^-, and $FeCl_4^-$).[9–12] The hydronium solvate IL intersects the solvate and protic types of IL, where protic H_3O^+ ion (i.e., solute) is solvated by 18C6 ligand (i.e., solvent) to form a $[H_3O^+{\cdot}18C6]$ complex cation (i.e., solvate) and Tf_2N^- as the counter anion. Its strong Brønsted acidity among ILs (Hammett acidity H_0 = –4.4 [8]) indicates that it may be used as an acid catalyst and in fuel cells.[6,13-20]

Moreover, the proton conduction of hydronium solvate ILs has been of special interest. Pulsed-field gradient spin echo nuclear magnetic resonance (PGSE-NMR) measurements revealed that protons of H_3O^+ move faster than those of 18C6 ligands in $[H_3O^+{\cdot}18C6]Tf_2N$.[21] Among solvate ILs and protic ILs,[22–25] this was the first observation of ligand exchange conduction without *free* neutral molecules. Further, unlike common solvate ILs and protic ILs, this cooperative proton relay is suppressed and H_3O^+ come to move as slow as 18C6 ligands when diluted using equimolar 18C6 solvent.[26] The proton conduction of the hydronium-based electrolytes would be interesting from the viewpoint of recently-proposed hydronium ion batteries[27,28] as well as fuel cells.[6,13–15]

In these studies, however, a key factor of the fast proton conduction has not been revealed. To understand the anomalous proton conduction, it is important to study analogous compounds with different ligands. Since 18C6 is a plausible ligand of H_3O^+ and a good acceptor that binds H_3O^+ cation selectively owing to its cavity size,[9–12,29] other candidate ligands are also cyclic or acyclic polyethers with six ether oxygens akin to 18C6.

In this work, three novel hydronium solvate ILs analogous to $[H_3O^+{\cdot}18C6]Tf_2N$ are synthesized and the proton conduction of these hydronium solvate ILs are studied. A set of ^1H PGSE-NMR measurements was performed to determine the self-diffusion coefficients of H_3O^+ and the ligands of the hydronium solvate ILs. The obtained results are also compared with density functional theory

[a] Department of Materials Science and Engineering, Kyoto University, Sakyo-ku, Kyoto 606-8501, Japan.
E-mail: kitada.atsushi.3r@kyoto-u.ac.jp; Tel.: +81-75-753-5475; Fax: +81-75-753-5463
[b] Institute of Advanced Energy, Kyoto University, Gokasho, Uji, Kyoto 611-0011, Japan.

†Electronic Supplementary Information (ESI) available: The lists of ionic conductivities and viscosities for each hydronium solvate IL. Graphical representation of the equilibrium geometry of the most stable conformers of two $[H_3O^+{\cdot}Dh18C6]$ cations and two $[H_3O^+{\cdot}B18C6]$ cations (B3LYP/6-311+G** level). See DOI: 10.1039/x0xx00000x

(DFT) calculations to reveal the distinguishable effect of ligand shape associated with cyclic or acyclic ligands on the proton conduction of hydronium solvate ILs.

Experimental

Materials.

Dicyclohexano-18-crown-6 (Dh18C6; Tokyo Chemical Industry Co., Ltd., >98.0% purity), benzo-18-crown-6 (B18C6; Tokyo Chemical Industry Co., Ltd., >96.0% purity), pentaethylene glycol dimethyl ether (G5; Nippon Nyukazai Co., 99.0% purity), and bis[(trifluoromethyl)sulfonyl]imide (HTf_2N; Kanto Chemical, 99% purity) were used without further purification. Ultrapure water was prepared using a Merck Milli-Q Reference A system.

Synthesis of hydronium solvate ILs.

We synthesized $[H_3O^+\cdot Dh18C6]Tf_2N$ and $[H_3O^+\cdot B18C6]Tf_2N$ in an Ar-filled glovebox using the methods reported in ref. 8 and 26, respectively. On the other hand, $[H_3O^+\cdot G5]Tf_2N$ was prepared in an Ar-filled glovebox as follows. Water was mixed with an equimolar amount of G5 in a septum-sealed vial at room temperature (RT), and then this mixture was added dropwise to HTf_2N at –10 °C.

Characterization of hydronium solvate ILs.

Melting points (T_m) and glass transition temperatures (T_g) were determined using a differential scanning calorimeter (DSC; Rigaku, DSC8231) at a heating rate of 5 °C min^{-1}. Proton nuclear magnetic resonance (^1H NMR) spectra for $[H_3O^+\cdot Dh18C6]Tf_2N$ at 60 °C, $[H_3O^+\cdot B18C6]Tf_2N$ at 75 °C, and $[H_3O^+\cdot G5]Tf_2N$ at 25 °C were obtained at 600 MHz using a JNM-ECA600 FT NMR spectrometer (JEOL Ltd.). The use of a double NMR tube, purchased from Shigemi Corp. (Catalog NO. SC-002), prevented the sample from mixing with the external standard. Traces of dimethyl sulfoxide-d_6 (Cambridge Isotope Laboratories, Inc.) were placed in the outer tube (5.2 mmϕ) and compounds were added to the internal tube (5.0 mmϕ).Thermal gravimetric analysis (TGA) was conducted for $[H_3O^+\cdot Dh18C6]Tf_2N$, $[H_3O^+\cdot B18C6]Tf_2N$, and $[H_3O^+\cdot G5]Tf_2N$ at a heating rate of 5 °C min^{-1}, using a TG-DTA8122 (Rigaku) instrument in a dry air atmosphere. Aluminum pans were used for the measurements. For each measurement, a 10 mg sample was placed on the pan and Al_2O_3 was used as a standard.

Ionic conductivity (σ) of the electrolyte was determined by electrochemical impedance spectroscopy for $[H_3O^+\cdot Dh18C6]Tf_2N$ from 50 °C to 90 °C, $[H_3O^+\cdot B18C6]Tf_2N$ from 60 °C to 85 °C, and $[H_3O^+\cdot G5]Tf_2N$ from 5 °C to 45 °C. A Bio-Logic Science Instruments SAS, VSP-300, was used with stainless steel electrodes. The cell constant was calibrated with 0.1 and 1 mol dm^{-3} KCl aqueous solutions. The measurement was conducted in a thermostatic chamber (Espec Co., SU-222). Viscosity (η) measurements were performed for each sample in the same temperature range as conductivity measurements using a viscometer (Kyoto Electronics Manufacturing Co., Ltd., EMS-1000). Using the measured values of weight and volume, densities (ρ) for each compound were calculated.

Proton PGSE-NMR measurements were also performed for $[H_3O^+\cdot Dh18C6]Tf_2N$ (at 70 °C), $[H_3O^+\cdot B18C6]Tf_2N$ (at 75 °C), and $[H_3O^+\cdot G5]Tf_2N$ (at 25 °C) by the same equipment used for NMR measurement. The self-diffusion coefficients of H_3O^+ and ligands (Dh18C6, B18C6, and G5) in these compounds were measured using

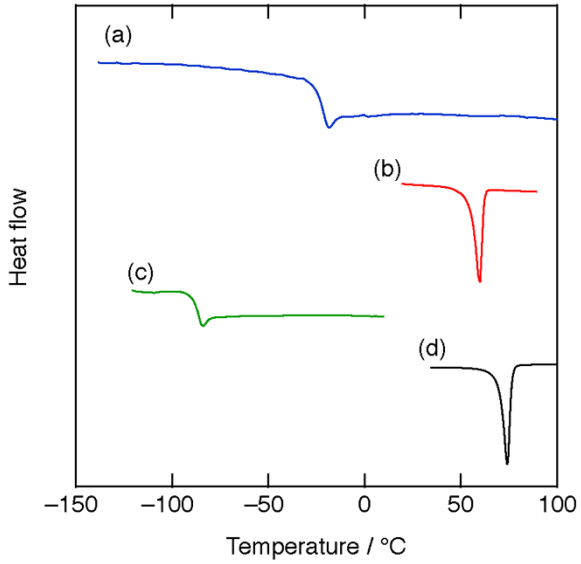

Fig. 1. DSC curves for (a) $[H_3O^+\cdot Dh18C6]Tf_2N$, (b) $[H_3O^+\cdot B18C6]Tf_2N$, (c) $[H_3O^+\cdot G5]Tf_2N$, and (d) $[H_3O^+\cdot 18C6]Tf_2N$ (ref. 8) at a heating rate of 5 °C min^{-1}.

Table 1 Physical properties of hydronium solvate ILs

Ideal composition and formula weight (g mol^{-1})	T_m or T_g (°C)	σ (mS cm^{-1})	η (mPa s)	ρ (g cm^{-3})
$[H_3O^+\cdot Dh18C6]Tf_2N$ (671.67)	T_g –24	0.58 at 70 °C	155.1 at 70 °C	1.31 at RT
$[H_3O^+\cdot B18C6]Tf_2N$ (611.53)	T_m 52–54	0.85 at 75 °C	106.8 at 75 °C	1.33 at 60 °C
$[H_3O^+\cdot G5]Tf_2N$ (565.51)	T_g –90	2.22 at 25 °C	50.2 at 25 °C	1.45 at 25 °C
[a] $[H_3O^+\cdot 18C6]Tf_2N$ (563.48)	T_m 66–68	2.36 at 75 °C	42.9 at 75 °C	1.32 at 70 °C

[a]Data for $[H_3O^+\cdot 18C6]Tf_2N$ are from ref. 8.

Table 2 Elemental analysis results for hydronium solvate ILs

Compound		H (%)	C (%)	N (%)	F (%)	S (%)
$[H_3O^+ \cdot Dh18C6]Tf_2N$	Experimental	5.77	38.68	2.13	17.21	9.70
	Calculated	5.85	39.34	2.09	16.97	9.55
$[H_3O^+ \cdot B18C6]Tf_2N$	Experimental	4.64	35.51	2.42	18.52	10.31
	Calculated	4.45	35.35	2.29	18.64	10.49
$[H_3O^+ \cdot G5]Tf_2N$	Experimental	5.33	29.52	2.45	20.13	11.29
	Calculated	5.17	29.74	2.48	20.16	11.34

a simple Hahn spin echo sequence and analyzed using the Stejskal equation:

$$\ln(I/I_0) = -D(\gamma g \delta)^2(\Delta - \delta/3),$$

where I is the echo signal intensity, I_0 is the initial echo signal intensity, D is the self-diffusion coefficient, γ is the gyromagnetic ratio (2.67515×10^8 rad s^{-1} T^{-1} for ^1H), g is the amplitude of the gradient pulses, δ is the duration of the gradient pulses, and Δ is the interval between the leading edges of the gradient pulses.[30] The g values used were in the range 20–270 mT m^{-1} for $[H_3O^+ \cdot Dh18C6]Tf_2N$ and 20–280 mT m^{-1} for $[H_3O^+ \cdot B18C6]Tf_2N$ and $[H_3O^+ \cdot G5]Tf_2N$. The value of δ was 4 ms for $[H_3O^+ \cdot Dh18C6]Tf_2N$ and 8 ms for $[H_3O^+ \cdot B18C6]Tf_2N$ and $[H_3O^+ \cdot G5]Tf_2N$, and Δ was 100 ms.

The Gaussian 16 program[31] was used for the ab initio molecular orbital calculations. The basis sets implemented in the Gaussian program were used. The geometry of 18C6, G5, Dh18C6, and B18C6 complexes with H_3O^+ was fully optimized at the B3LYP/6-311+G** level. Additionally, to investigate the degree of orientation for two cation complexes, the geometry of two $[H_3O^+ \cdot (ligand)]$ (ligand=18C6 and G5) was also fully optimized at the B3LYP/6-311+G** level under tetrahydrofuran atmosphere, because the dielectric permittivity is similar to that of common ILs.[32]

Results and discussion

Characterization of hydronium solvate ILs.

Both an equimolar mixture made of Dh18C6, HTf_2N, and H_2O, i.e., $[H_3O^+ \cdot Dh18C6]Tf_2N$, and that made of G5, HTf_2N, and H_2O, i.e., $[H_3O^+ \cdot G5]Tf_2N$, were yellowish liquids, while that made of B18C6, HTf_2N, and H_2O, i.e., $[H_3O^+ \cdot B18C6]Tf_2N$, was a white solid at RT. The DSC curves for these compounds are shown in Fig. 1, and their melting points T_m or glass transition points T_g are listed in Table 1. All samples have melting points below 100 °C, satisfying the fourth criterion of solvate ILs.[8,33] In Fig. 1, no peaks are seen near the melting points of pure ligands nor that of HTf_2N. Therefore, these compounds

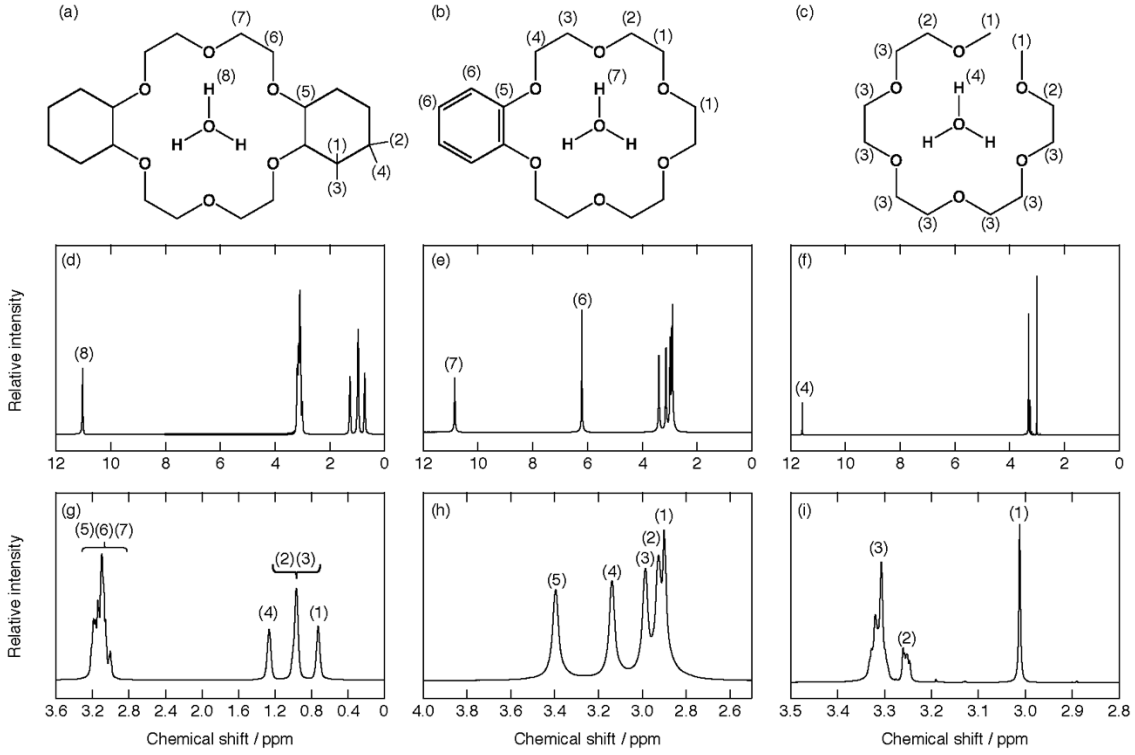

Fig. 2. (a-c) Schematic cation structure of (a) $[H_3O^+ \cdot Dh18C6]$, (b) $[H_3O^+ \cdot B18C6]$, and (c) $[H_3O^+ \cdot G5]$; (d-f) ^1H NMR spectra; (g-i) enlarged plots for (d,g) $[H_3O^+ \cdot Dh18C6]Tf_2N$ at 60 °C, (e,h) $[H_3O^+ \cdot B18C6]Tf_2N$ at 75 °C, and (f,i) $[H_3O^+ \cdot G5]Tf_2N$ at 25 °C.

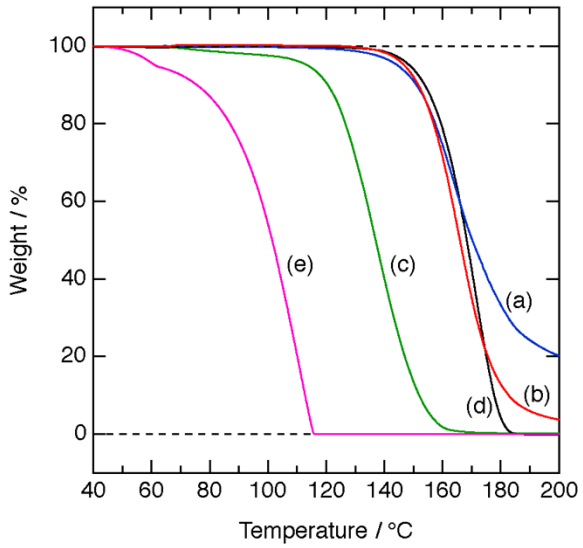

Fig. 3. TGA curves at a heating rate of 5 °C min^{-1}; (a) $[H_3O^+\cdot Dh18C6]Tf_2N$, (b) $[H_3O^+\cdot B18C6]Tf_2N$, (c) $[H_3O^+\cdot G5]Tf_2N$, (d) $[H_3O^+\cdot 18C6]Tf_2N$, and (e) $HTf_2N\cdot H_2O$ (a–c: this work, e: ref. 8, f: ref. 26).

show no physicochemical properties based on both pure ligands and precursor salts, satisfying the third criterion of solvate ILs.[8,33]

Table 2 shows the elemental analysis data for H, C, N, F, and S content of each mixture, which was performed at the center for Organic Elemental Microanalysis, Kyoto University. Oxygen atoms cannot be analyzed in principle of the elemental analysis. The data were consistent with the suggested formulations $[H_3O^+\cdot Dh18C6]Tf_2N$, $[H_3O^+\cdot B18C6]Tf_2N$, and $[H_3O^+\cdot G5]Tf_2N$. The H_2O contents, as analyzed by Karl-Fischer coulometric titration of $[H_3O^+\cdot Dh18C6]Tf_2N$, $[H_3O^+\cdot B18C6]Tf_2N$, and $[H_3O^+\cdot G5]Tf_2N$, were 2.61, 3.03, and 3.20 wt%, which are in good agreement with the calculated values for each sample (2.68 wt% for $[H_3O^+\cdot Dh18C6]Tf_2N$, 2.94 wt% for $[H_3O^+\cdot B18C6]Tf_2N$, and 3.18 wt% for $[H_3O^+\cdot G5]Tf_2N$). These quantitative analyses support that each complex had a ligand to HTf_2N to H_2O molar ratio of 1:1:1, suggesting that all the mixtures in this study form a solvate compound between an ion and a ligand in a certain stoichiometric ratio. This satisfies the first criterion of solvate ILs.[8,33]

Figure 2 exhibits the schematic structure of the cations and the ^{1}H NMR spectra for the hydronium solvate ILs. The assignment of NMR signals for H_3O^+, Dh18C6, B18C6, and G5 are also displayed in each spectrum. The signals from H_3O^+ in $[H_3O^+\cdot Dh18C6]Tf_2N$, $[H_3O^+\cdot B18C6]Tf_2N$, and $[H_3O^+\cdot G5]Tf_2N$ appear at 11.03, 10.86, and 11.58 ppm, respectively. As reported previously,[8] in $[H_3O^+\cdot 18C6]Tf_2N$, where unprotonated water is excluded and H_3O^+ is solvated by 18C6 ligands, the chemical shift of the H_3O^+ NMR signal is 10.85 ppm. As also discussed in our previous report,[21] one ^{1}H NMR singlet is observed at 8.18 ppm in an equimolar mixture of H_2O and HTf_2N ($HTf_2N\cdot H_2O$), where its degree of dissociation is low and unprotonated H_2O exists to some extent. Every H_3O^+ signal in the compounds of this study is comparable to that of $[H_3O^+\cdot 18C6]Tf_2N$. Thus, these signals correspond to H_3O^+ solvated by ligand, satisfying

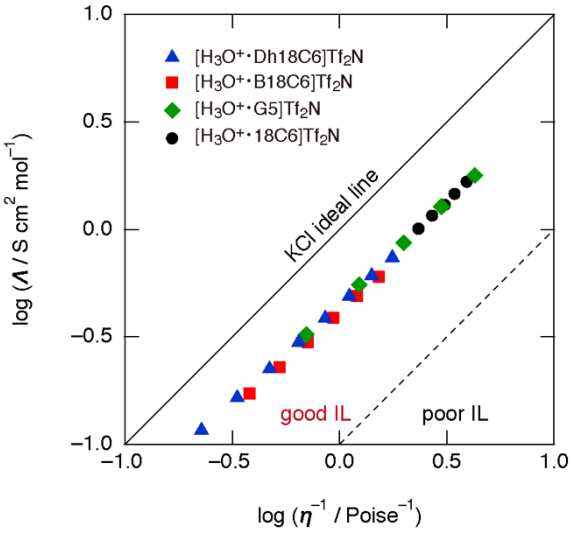

Fig. 4. Walden plots for $[H_3O^+\cdot Dh18C6]Tf_2N$, $[H_3O^+\cdot B18C6]Tf_2N$, $[H_3O^+\cdot G5]Tf_2N$, and $[H_3O^+\cdot 18C6]Tf_2N$ (ref. 8).

the second criterion of solvate ILs.[8,33] Further, we can consider all NMR signals of each ligand to be from bound molecules, hence there are no physicochemical properties based on pure ligand. This supports the DSC results.

In TGA data (Fig. 3) with a heating rate of 5 °C min^{-1}, $[H_3O^+\cdot Dh18C6]Tf_2N$, $[H_3O^+\cdot B18C6]Tf_2N$, and $[H_3O^+\cdot G5]Tf_2N$ start volatilizing at a much higher temperature than $HTf_2N\cdot H_2O$ does, as is the case for $[H_3O^+\cdot 18C6]Tf_2N$.[8] More precisely, 5 wt% loss is detected at around 150 °C for $[H_3O^+\cdot Dh18C6]Tf_2N$ and $[H_3O^+\cdot B18C6]Tf_2N$, similar to the behavior of $[H_3O^+\cdot 18C6]Tf_2N$, while for $[H_3O^+\cdot G5]Tf_2N$ it occurs at 110 °C. The vapor pressures of $[H_3O^+\cdot Dh18C6]Tf_2N$, $[H_3O^+\cdot B18C6]Tf_2N$, and $[H_3O^+\cdot G5]Tf_2N$ are negligible at temperatures lower than 100 °C, satisfying the fifth criterion of solvate ILs.[8,33]

The DSC, ^{1}H NMR results, and elemental analysis suggest that compounds synthesized in this work consist of H_3O^+ solvated by ligand (Dh18C6, B18C6, and G5) and Tf_2N^-. Additionally, the TGA clarifies that $[H_3O^+\cdot Dh18C6]Tf_2N$, $[H_3O^+\cdot B18C6]Tf_2N$, and $[H_3O^+\cdot G5]Tf_2N$ have low volatility under 100 °C. Therefore, $[H_3O^+\cdot Dh18C6]Tf_2N$, $[H_3O^+\cdot B18C6]Tf_2N$, and $[H_3O^+\cdot G5]Tf_2N$ are classified as solvate ILs according to the criteria,[33] as well as the original hydronium solvate IL $[H_3O^+\cdot 18C6]Tf_2N$.[8]

Physical properties (ionic conductivity σ, viscosity η, and density ρ) of $[H_3O^+\cdot Dh18C6]Tf_2N$, $[H_3O^+\cdot B18C6]Tf_2N$, $[H_3O^+\cdot G5]Tf_2N$, and $[H_3O^+\cdot 18C6]Tf_2N$ are summarized in Table 1. In addition, ionic

Table 3 The activation energy (kJ mol^{-1}) for ionic conductivity and viscosity

compound	ionic conductivity	viscosity
$[H_3O^+\cdot Dh18C6]Tf_2N$	54.2	60.1
$[H_3O^+\cdot B18C6]Tf_2N$	49.9	55.0
$[H_3O^+\cdot G5]Tf_2N$	31.4	33.2
[a] $[H_3O^+\cdot 18C6]Tf_2N$	28.0	28.9

[a]Data for $[H_3O^+\cdot 18C6]Tf_2N$ are from ref. 8.

conductivities and viscosities for each hydronium solvate IL are listed in Tables S1, S2, and S3. A plot of molar conductivity (Λ / S cm^2 mol^{-1}) vs. fluidity (η^{-1} / Poise^{-1}; 1 Poise = 0.1 Pa s), i.e., the Walden plot, is displayed in Fig. 4. The plot reveals that all compounds synthesized in this work are categorized as "good ILs" as well as $[H_3O^+\cdot 18C6]Tf_2N$ and common ILs.[8,33-35] The activation energy for ionic conductivity and viscosity estimated from Arrhenius plots are listed in Table 3. Similar to $[H_3O^+\cdot 18C6]Tf_2N$,[8] the activation energy of all the compounds in this work for ionic conductivity is somewhat smaller than that for viscosity.

Proton conduction of hydronium solvate ILs.

The PGSE-NMR results in Fig. 5 show plots of echo signal attenuation based on the Stejskal equation for H_3O^+ (black circles) and ligand (red circles) of $[H_3O^+\cdot Dh18C6]Tf_2N$ at 70 °C, $[H_3O^+\cdot B18C6]Tf_2N$ at 75 °C, $[H_3O^+\cdot G5]Tf_2N$ at 25 °C, and $[H_3O^+\cdot 18C6]Tf_2N$ at 75 °C.[21] As shown, the plots are linear. According to the Stejskal equation, the gradients of the fitted lines are proportional to the diffusion coefficients. Table 4 lists the estimated values of the self-diffusion coefficients for $[H_3O^+\cdot Dh18C6]Tf_2N$, $[H_3O^+\cdot B18C6]Tf_2N$, $[H_3O^+\cdot G5]Tf_2N$, and previously reported $[H_3O^+\cdot 18C6]Tf_2N$.[21] As in $[H_3O^+\cdot 18C6]Tf_2N$, the diffusion coefficients of H_3O^+ are larger than those of the ligands (Dh18C6 and B18C6) in $[H_3O^+\cdot Dh18C6]Tf_2N$ and $[H_3O^+\cdot B18C6]Tf_2N$, respectively. For $[H_3O^+\cdot G5]Tf_2N$, in contrast, the coefficients of H_3O^+ and G5 are very similar, as in common Li-glyme based solvate ILs where the diffusion coefficient ratio of glyme to Li falls into the range 0.9–1.1.[35] Consequently, protons of H_3O^+ move faster than ligands in $[H_3O^+\cdot Dh18C6]Tf_2N$ and $[H_3O^+\cdot B18C6]Tf_2N$ as in the case of $[H_3O^+\cdot 18C6]Tf_2N$, while they move as fast as ligands in $[H_3O^+\cdot G5]Tf_2N$. That is to say, the fast proton conduction is observed in all cyclic-ligand-based hydronium solvate ILs, while it was not observed in acyclic-ligand-based one. Note that in $[H_3O^+\cdot Dh18C6]Tf_2N$ the H_2O content analyzed by Karl-Fischer titration (2.61 wt%) is somewhat smaller than the calculated value (2.68 wt%) as above. Therefore, it is not the case that a little extra

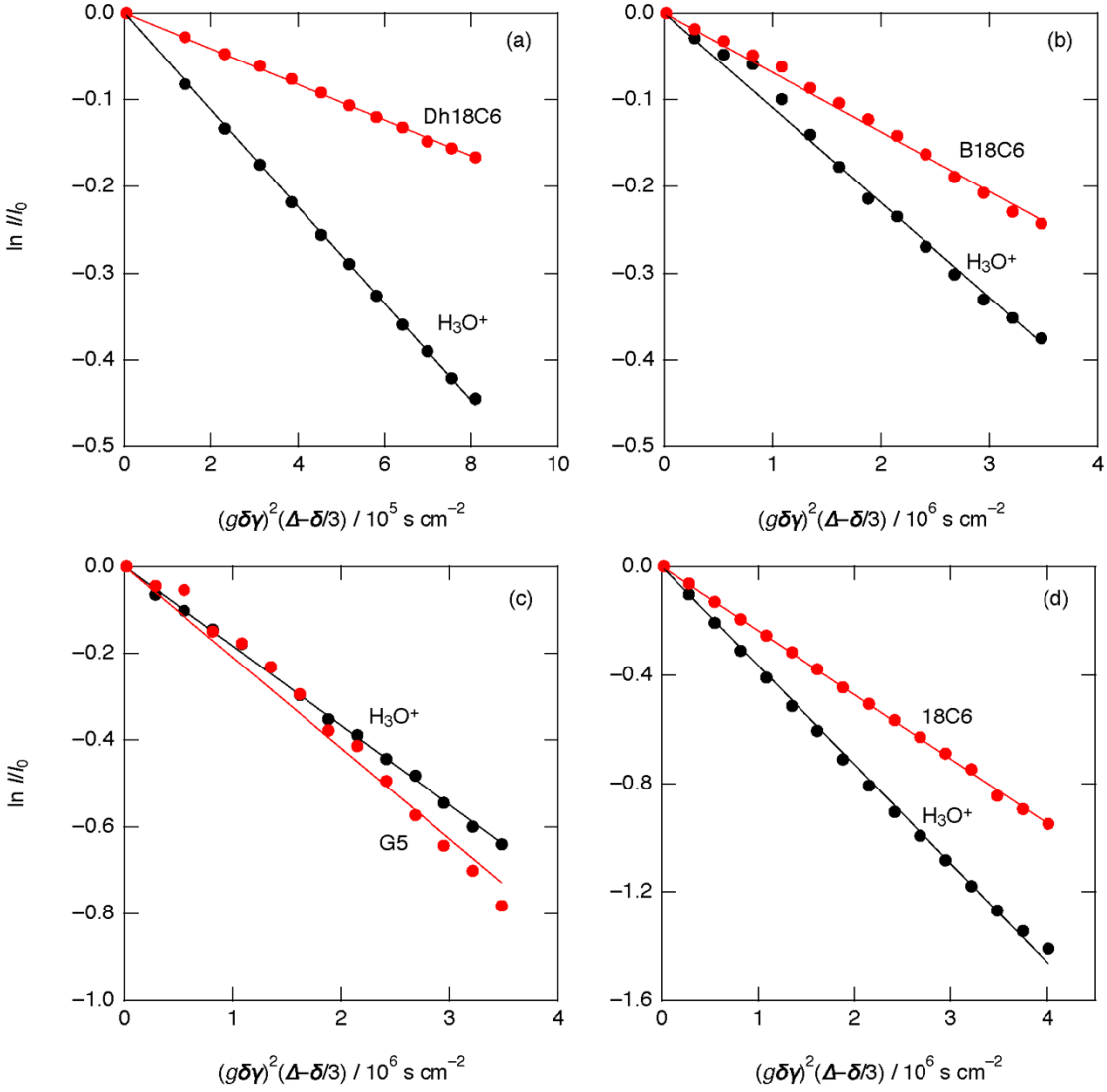

Fig. 5. Plots and best-fit lines of echo signal attenuation based on the Stejskal equation for (a) $[H_3O^+\cdot Dh18C6]Tf_2N$ at 70 °C, (b) $[H_3O^+\cdot B18C6]Tf_2N$ at 75 °C, (c) $[H_3O^+\cdot G5]Tf_2N$ at 25 °C, and (d) $[H_3O^+\cdot 18C6]Tf_2N$ at 75 °C (ref. 21): ligand (red circles) and H_3O^+ (black circles).

Table 4 Diffusion coefficients of H_3O^+ and ligand for hydronium solvate ILs

compound	Temp. [°C]	$D_{H_3O^+}$ [10^{-7} cm^2 s^{-1}]	D_{ligand} [10^{-7} cm^2 s^{-1}]	$D_{H_3O^+}$/ D_{ligand}
$[H_3O^+ \cdot Dh18C6]Tf_2N$	70	0.56	0.21	2.7
$[H_3O^+ \cdot B18C6]Tf_2N$	75	1.1	0.69	1.6
$[H_3O^+ \cdot G5]Tf_2N$	25	1.8	2.1	0.88
[a] $[H_3O^+ \cdot 18C6]Tf_2N$	75	3.6	2.4	1.5

[a]Data for $[H_3O^+ \cdot 18C6]Tf_2N$ are from ref. 21.

water in hydronium solvate ILs assists the cooperative proton relay. It is also notable that the activation energy for ionic conductivity is smaller than that for viscosity, not only in $[H_3O^+ \cdot Dh18C6]Tf_2N$ and $[H_3O^+ \cdot B18C6]Tf_2N$ but also in $[H_3O^+ \cdot G5]Tf_2N$.

To discuss the difference of proton conduction between cyclic-ether-based hydronium solvate ILs and acyclic one from a structural viewpoint, graphical representations of the equilibrium geometry of the most stable conformers of $[H_3O^+ \cdot 18C6]$ and $[H_3O^+ \cdot G5]$ are displayed in Figs. 6a and b, respectively. In the former case, every other oxygen atom of 18C6 coordinates to the H_3O^+, forming highly symmetric coordination via three equivalent hydrogen bonds, which agrees with some pioneering works,[36–38] and so do those of both Dh18C6 and B18C6 (Figure S1, S2). In the latter case, G5 does not wrap around the H_3O^+ cation completely, and the first to fourth of the six oxygen atoms of G5 participate in coordination to the H_3O^+. A $[H_3O^+ \cdot G5]$ complex does not form an 18C6-like coordination geometry but instead forms an asymmetric structure. These discussions are supported by the fact that $[H_3O^+ \cdot G5]Tf_2N$ undergoes glass transition at –90 °C while $[H_3O^+ \cdot 18C6]Tf_2N$ crystalizes at 66–68 °C, although the molar weights of the two compounds are almost the same. Consequently, the degree of structural freedom of G5 is larger than that of the 18C6-based ligand because G5 is an acyclic, open-chain ligand.

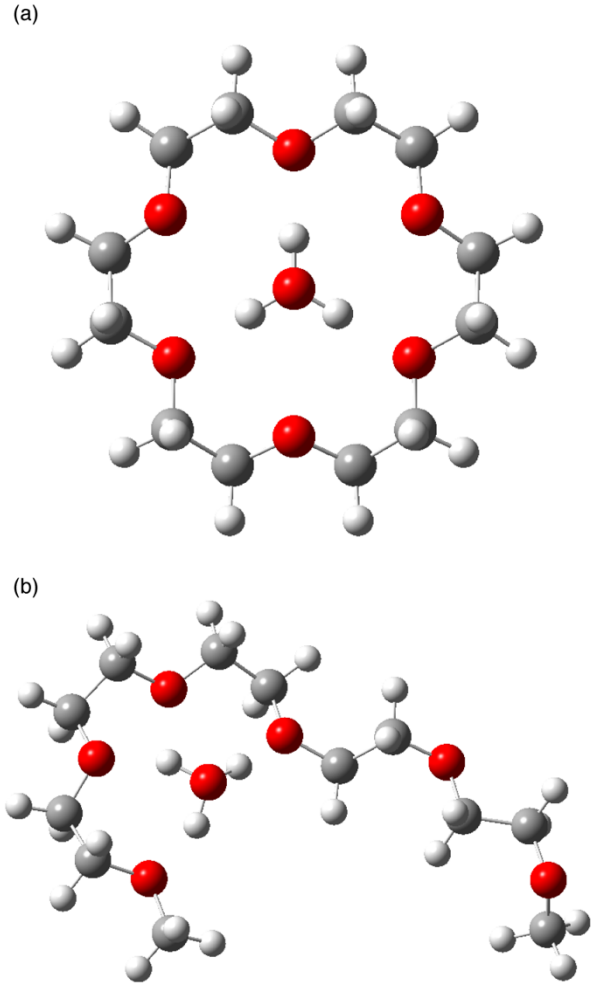

Fig. 6. Graphical representation of the equilibrium geometry of the most stable conformers of (a) 18C6 complexes with H_3O^+ (B3LYP/6-311+G** level) and (b) G5 complexes with H_3O^+ (B3LYP/6-311+G** level): oxygens in red, carbons in gray, and hydrogens in white.

In common protic ILs, reorientation of a proton acceptor is required for the fast proton transfer.[39] Although the proton transfer mechanism differs between hydronium solvate ILs and common protic ILs —in that the former does not include excess neutral molecules that can help proton relay—, we consider that ligand

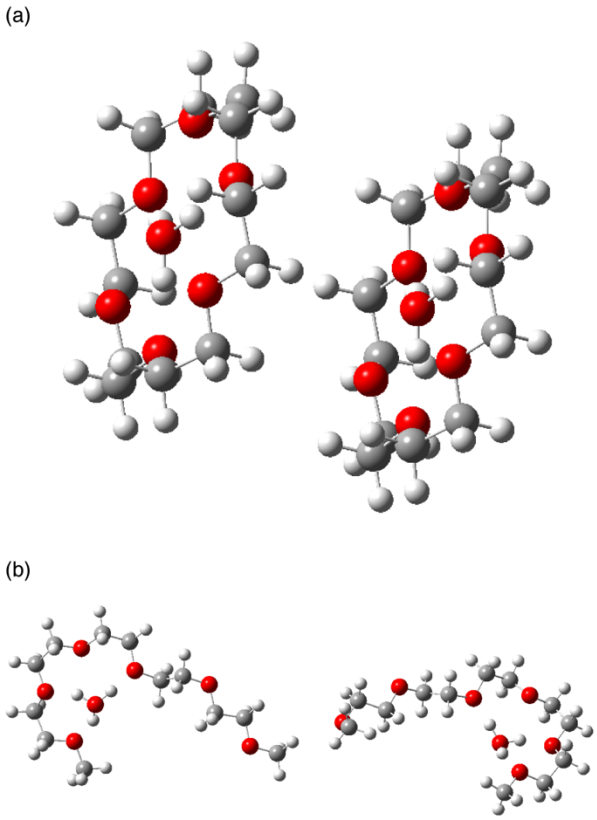

Fig. 7. Graphical representation of the equilibrium geometry of the most stable conformers of (a) two $[H_3O^+ \cdot 18C6]$ cations and (b) two $[H_3O^+ \cdot G5]$ cations (B3LYP/6-311+G** level): oxygens in red, carbons in gray, and hydrogens in white.

reorientation is also needed for the fast proton conduction in hydronium solvate ILs. In fact, the optimized structure of two solvate cations, which is performed to investigate their degree of orientation, clearly show that the pairs of [H_3O^+·18C6] face each other (Figure 7a), while two [H_3O^+·G5] do not (Fig. 7b). In the system like biological ion channel, where ions pass through the specific path, ligands are needed to line up in parallel. A solid system where crown ether stacks are known as an artificial analogue of such ion channel.[40] In the hydronium solvate ILs, where solvate cations and anions move relative to each other, the solvate cations will not stay and stack at specific area. Nonetheless, whether the ligands face each other frequently or not, i.e. whether the ligand reorientation occurs frequently, is important for the proton conduction. That is, the results shown in Fig. 7 strongly indicate the large difference in the probabilities of ligand reorientation for the crown ether and the glyme solvates. In [H_3O^+·G5]Tf_2N, fast proton conduction has *not* been found, evidencing that states in which two [H_3O^+·G5] face each other are infrequent. Certainly, the open G5 ligand is more flexible than the closed 18C6-based ligands. However, G5 cannot maintain the specific states of ligand orientation required for the fast proton conduction due to its high flexibility, which may suppress fast proton conduction. In contrast, the ligand reorientation occurs frequently for the 18C6-based ligands owing to its rigidity. As a result, conduction paths are available for a cooperative proton relay and fast proton conduction takes place.

Here we further discuss why such different proton conduction is observed in the cyclic- and acyclic-ligand-based hydronium solvate ILs. Crown ethers show amphiphilicity because of the hydrophobic –CH_2CH_2– groups and the hydrophilic inherent ether oxygens. The ether oxygens are well situated to coordinate with a cation located at the interior of the ring, whereas the exterior of the ring is hydrophobic. The cyclic molecules can divide hydrophilic area and hydrophobic area due to its closed nature. Therefore, the fast proton conduction appears in cyclic-ligand-based hydronium solvate ILs. Especially, Dh18C6 shows more exterior hydrophobicity than 18C6 owing to two cyclohexane moieties, resulting larger ratio of diffusion coefficients of H_3O^+ and ligand in [H_3O^+·Dh18C6]Tf_2N than in [H_3O^+·18C6]Tf_2N. Apparently, B18C6 also shows exterior hydrophobicity compared to 18C6. Benzene ring, however, is known not only as a hydrophobic solute but also as a hydrogen bond acceptor.[41] As a result, the ratio of diffusion coefficients of H_3O^+ and ligand is almost the same in [H_3O^+·B18C6]Tf_2N and in [H_3O^+·18C6]Tf_2N. On the other hand, glyme molecules can also show both hydrophobicity and hydrophilicity. The two properties, however, cannot completely be interior/exterior for such open-chain and flexible molecules. Thus, it is the closed nature of crown ether or "partitioned amphiphilicity" that gives conduction paths for the cooperative proton relay. In [H_3O^+·G5]Tf_2N, such conduction paths for cooperative proton relay are not available. It may be notable that hydronium solvate ILs may relate to the ionics in biological ion channels. By utilizing crown ethers, artificial ion channels have widely been studied,[40,42–47] where hydrophilic ion channel in hydrophobic lipid bilayer is mimicked. Although these studies focus on ion selectivity and ion transport, as far as we know, the effect of the partitioned amphiphilicity on the ionics by comparing the ligand structure has not been reported.

Consequently, the proton conduction of cyclic-ligand-based hydronium solvate ILs and that of acyclic counterpart are different. The DFT calculations show that the rigidity of 18C6 allows two [H_3O^+·18C6] cations to be parallel, implying small ligand reorientation, while two [H_3O^+·G5] cations are not. Therefore, the fast proton conduction only appears in cyclic-ligand-based hydronium solvate ILs. Additionally, since the conduction carrier is protons of H_3O^+ or H_3O^+ itself in hydronium solvate ILs, the hydrophilic area of ligand plays a role as proton acceptor. The hydrophilic and hydrophobic area of cyclic ligand can be divided owing to its closed nature, while those of acyclic one cannot because it is open chain. Therefore, we propose that the topology of the ethereal ligands is a clue for the proton conduction of hydronium solvate ILs.

Conclusions

The dependence of ligand shape on the proton conduction in hydronium solvate ILs was studied. While protons of H_3O^+ move faster than the cyclic 18C6-based ligands, such fast proton conduction was not observed in the case of acyclic G5 ligands. Consequently, whether H_3O^+ ion is coordinated by cyclic or acyclic ligands — in other words, whether H_3O^+ wears a "crown" or "tiara" — is a key factor for proton conduction in hydronium solvate ILs, and the "coronation" or the crown-ether coordination matters. These findings should reflect the topological difference of the ethereal ligands. For further studies, molecular dynamics simulations for these hydronium solvate ILs, which would detect temporal ion channels in liquids, are of special interest. Our findings can provide guidelines to design new electrolyte systems for fuel cells and artificial ion channels for biological cells.

Conflicts of interest

There are no conflicts to declare.

Acknowledgements

The authors acknowledge Prof. Yasuhiro Umebayashi (Niigata University) for his support with the DFT calculations. This work was supported financially by Grants-in-Aid for Grants-in-Aid for Scientific Research (S) (No. 20H05663: K. M.), Scientific Research (B) (No. 19H02490: A. K.) and Grant-in-Aid for Challenging Research (Exploratory) (No. 19K22056: A. K.) from the Japan Society for the Promotion of Science. A. K. also thanks the Joint Usage/Research Program on Zero-Emission Energy Research, Institute of Advanced Energy, Kyoto University (ZE31A-1 and ZE2020A-09).

References

1 T. Welton, *Chem. Rev.*, 1999, **99**, 2071-2083.
2 K. Fujita, K. Murata, M. Masuda, N. Nakamura, and H. Ohno, *RSC Adv.*, 2012, **2**, 4018-4030.
3 T. L. Greaves and C. J. Drummond, *Chem. Rev.*, 2015, **115**, 11379-11448.

4 P. A. Hunt, C. R. Ashworth, and R. P. Matthews, *Chem. Soc. Rev.*, 2015, **44**, 1257-1288.
5 M. Armand, F. Endres, D. R. MacFarlane, H. Ohno, and B. Scrosati, *Nat. Mater.*, 2009, **8**, 621-629.
6 A. S. Amarasekara, *Chem. Rev.*, 2016, **116**, 6133-6183.
7 C. A. Angell, Y. Ansari, and Z. Zhao, *Faraday Discuss.*, 2012, **154**, 9-27.
8 A. Kitada, S. Takeoka, K. Kintsu, K. Fukami, M. Saimura, T. Nagata, M. Katahira, and K. Murase, *J. Electrochem. Soc.*, 2018, **165**, H121-H127.
9 G. S. Heo and R. A. Bartsch, *J. Org. Chem.*,1982, **47**, 3557-3559.
10 R. Chênevert, A. Rodrigue, P. Beauchesne, and R. Savoie, *Can. J. Chem.*, 1984, **62**, 2293-2298.
11 R. Chênevert and A. Rodrique, *J. Chem. Educ.*, 1984, **61**, 465-466.
12 R. Chênevert, D. Chamberland, M. Simard, and F. Brisse, *Can. J. Chem.*, 1989, **67**, 32-36.
13 T. Yasuda and M. Watanabe, *MRS Bull.*, 2013, **38**, 560-566.
14 J. Gao, G. Wang, Z. Wang, Y. Wang, J. Liu, W. Liu, and Z. Zou, *J. Mater. Chem. A*, 2014, **2**, 19275-19281.
15 C. Ke, J. Li, X. Li, Z. Shao, and B. Yi, *RSC Adv.*, 2012, **2**, 8953-8956.
16 C. Chiappe and S. Rajamani, *Eur. J. Org. Chem.*, 2011, **2011**, 5517-5539.
17 R. Skoda-Földes, *Molecules*, 2014, **19**, 8840-8884.
18 Z. Duan, Y. Gu, J. Zhang, L. Zhu, and Y. Deng, *J. Mol. Catal. A: Chem.*, 2006, **250**, 163-168.
19 Y. L. Geng, L. Y. Hu, X. Q. Zhao, H. L. An, and Y. J. Wang, *Chin. J. Chem. Eng.*, 2009, **17**, 756-760.
20 H. Xing, T. Wang, Z. Zhou, and Y. Dai, *J. Mol. Catal. A: Chem.*, 2007, **264**, 53-59.
21 A. Kitada, K. Kintsu, S. Takeoka, K. Fukami, M. Saimura, T. Nagata, M. Katahira, and K. Murase, *J. Electrochem. Soc.*, 2018, **165**, H496-H499.
22 K. Yoshida, M. Nakamura, Y. Kazue, N. Tachikawa, S. Tsuzuki, S. Seki, K. Dokko, and M. Watanabe, *J. Am. Chem. Soc.*, 2011, **133**, 13121-13129.
23 M. A. B. H. Susan, A. Noda, S. Mitsushima, and M. Watanabe, *Chem. Commun*., 2003, 938-939.
24 A. Noda, M. A. B. H. Susan, K. Kudo, S. Mitsushima, K. Hayamizu, and M. Watanabe, *J. Phys. Chem. B*, 2003, **107**, 4024-4033.
25 H. Doi, X. Song, B. Minofar, R. Kanzaki, T. Takamuku, and Y. Umebayashi, *Chem. Eur. J.*, 2013, **19**, 11522-11526.
26 K. Kawata, A. Kitada, N. Tsuchida, M. Saimura, T. Nagata, M. Katahira, K. Fukami, and K. Murase, *J. Electrochem. Soc.*, 2020, **167**, 046508.
27 X. Wang, C. Bommier, Z. Jian, Z. Li, R. S. Chandrabose, I. A. Rodríguez-Pérez, P. A. Greaney, and X. Ji, *Angew. Chem. Int. Ed.*, 2017, **56**, 2909-2913.
28 Y. Zhu, X. Yang, and X. Zhang, *Angew. Chem. Int. Ed.*, 2017, **56**, 6378-6380.
29 P. C. Junk, *New J. Chem.*, 2008, **32**, 762-773.
30 E. O. Stejskal and J. E. Tanner, *J. Chem. Phys*., 1965, **42**, 288-292.
31 M. J. Frisch, G. W. Trucks, H. B. Schlegel, G. E. Scuseria, M. A. Robb, J. R. Cheeseman, G. Scalmani, V. Barone, G. A. Petersson, H. Nakatsuji, X. Li, M. Caricato, A. V. Marenich, J. Bloino, B. G. Janesko, R. Gomperts, B. Mennucci, H. P. Hratchian, J. V. Ortiz, A. F. Izmaylov, J. L. Sonnenberg, D. Williams-Young, F. Ding, F. Lipparini, F. Egidi, J. Goings, B. Peng, A. Petrone, T. Henderson, D. Ranasinghe, V. G. Zakrzewski, J. Gao, N. Rega, G. Zheng, W. Liang, M. Hada, M. Ehara, K. Toyota, R. Fukuda, J. Hasegawa, M. Ishida, T. Nakajima, Y. Honda, O. Kitao, H. Nakai, T. Vreven, K. Throssell, J. A. Montgomery, Jr., J. E. Peralta, F. Ogliaro, M. J. Bearpark, J. J. Heyd, E. N. Brothers, K. N. Kudin, V. N. Staroverov, T. A. Keith, R. Kobayashi, J. Normand, K. Raghavachari, A. P. Rendell, J. C. Burant, S. S. Iyengar, J. Tomasi, M. Cossi, J. M. Millam, M. Klene, C. Adamo, R. Cammi, J. W. Ochterski, R. L. Martin, K. Morokuma, O. Farkas, J. B. Foresman, D. J. Fox, *Gaussian 16, Revision A.03*, Gaussian Inc., Wallingford CT, 2016.
32 C. Daguenent, P. J. Dyson, I. Krossing, A. Oleinikova, J. Slattery, C. Wakai, and H. Weingärtner, *J. Phys. Chem. B*, 2006, **110**, 12682-12688.
33 T. Mandai, K. Yoshida, K. Ueno, K. Dokko, and M. Watanabe, *Phys. Chem. Chem. Phys.*, 2014, **16**, 8761-8772.
34 A. Kitada, D. Ishikawa, K. Fukami, and K. Murase, *J. Electrochem. Soc.*, 2017, **164**, H5119-H5123.
35 K. Ueno, K. Yoshida, M. Tsuchiya, N. Tachikawa, K. Dokko, and M. Watanabe, *J. Phys. Chem. B*, 2012, **116**, 11323-11331.
36 M. Bühl and G. Wipff, *J. Am. Chem. Soc.*, 2002, **124**, 4473-4480.
37 A. Varnek, G. Wipff, A. Famulari, M. Raimondi, T. Vorob'eva, and E. Stoyanov, *J. Chem. Soc., Perkin. Trans. 2*, 2002, 887-893.
38 M. Bühl, R. Ludwig, R. Schurhammer, and G. Wipff, *J. Phys. Chem. A*, 2004, **108**, 11463-11468.
39 M. L. Hoarfrost, M. Tyagi, R. A. Segalman, and J. A. Reimer, *J. Phys. Chem. B*, 2012, **116**, 8201-8209.
40 K. M. Fromm and R. D. Bergougnant, *Solid State Sci.*, 2007, **9**, 580-587.
41 T. R. Raschke and M. Levitt, *J. Phys. Chem. B*, 2004, **108**, 13492-13500.
42 V. E. Carmichael, P. J. Dutton, T. M. Fyles, T. D. James, J. A. Swan, and M. Zojaji, *J. Am. Chem. Soc.*, 1989, **111**, 767-769.
43 M. F. M. Roks and R. J. M. Nolte, *Macromolecules*, 1992, **25**, 5398-5407.
44 A. Cazacu, C. Tong, A. van der Lee, T. M. Fyles, and M. Barboiu, *J. Am. Chem. Soc.*, 2006, **128**, 9541-9548.
45 T. Liu, C. Bao, H. Wang, L. Fei, R. Yang, Y. Long, and L. Zhu, *New J. Chem.*, 2014, **38**, 3507-3513.
46 T. M. Fyles, T. D. James, and K. C. Kaye, *J. Am. Chem. Soc.*, 1993, **115**, 12315-12321.
47 Z. Sun, M. Barboiu, Y. -M. Legrand, E. Petit, and A. Rotaru, *Angew. Chem.*, 2015, **127**, 14681-14685.

Electronic Supplementary Information (ESI)

Proton conduction in hydronium solvate ionic liquids affected by ligand shape

Kio KAWATA,[a] Atsushi KITADA,[a,*] Naoki TSUCHIDA,[a] Masayuki SAIMURA,[b] Takashi NAGATA,[b] Masato KATAHIRA,[b] Kazuhiro FUKAMI,[a] and Kuniaki MURASE[a]

[a]*Department of Materials Science and Engineering, Kyoto University, Sakyo-ku, Kyoto 606-8501, Japan*

[b]*Institute of Advanced Energy, Kyoto University, Gokasho, Uji, Kyoto 611-0011, Japan*

[*]Corresponding author: kitada.atsushi.3r@kyoto-u.ac.jp

Table S1. Ionic conductivities and viscosities of $[H_3O^+ \cdot Dh18C6]Tf_2N$ at various temperatures.

Temperature (°C)	Conductivity (mS cm^{-1})	Viscosity (mPa s)
50	0.15	677
55	0.23	440
60	0.32	300
65	0.44	212
70	0.58	155
75	0.75	117
80	0.95	90.0
85	1.2	70.8
90	1.4	56.7

Table S2. Ionic conductivities and viscosities of $[H_3O^+ \cdot B18C6]Tf_2N$ at various temperatures.

Temperature (°C)	Conductivity (mS cm^{-1})	Viscosity (mPa s)
60	0.37	263
65	0.50	190
70	0.65	140
75	0.85	107
80	1.1	83.1
85	1.3	65.7

Table S3. Ionic conductivities and viscosities of $[H_3O^+ \cdot G5]Tf_2N$ at various temperatures.

Temperature (°C)	Conductivity (mS cm^{-1})	Viscosity (mPa s)
5	0.83	143
15	1.4	81.0
25	2.2	50.2
35	3.3	33.5
45	4.6	23.4

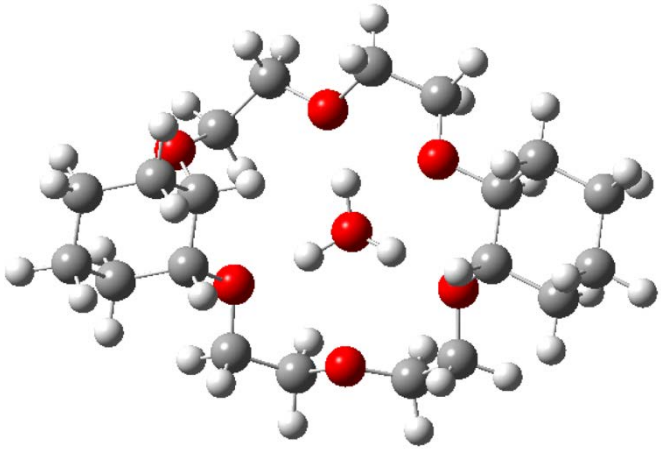

Fig. S1 Graphical representation of the equilibrium geometry of the most stable conformers of Dh18C6 complexes with H_3O^+ (B3LYP/6-311+G** level): oxygens in red, carbons in gray, and hydrogens in white.

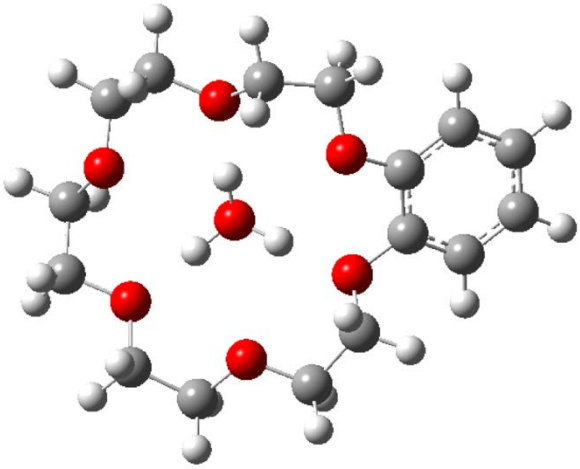

Fig. S2 Graphical representation of the equilibrium geometry of the most stable conformers of B18C6 complexes with H_3O^+ (B3LYP/6-311+G** level): oxygens in red, carbons in gray, and hydrogens in white.